PTEP

Prog. Theor. Exp. Phys. **2013**, 043D02 (18 pages)
DOI: 10.1093/ptep/ptt009

Production of hyperon resonances induced by kaons on a deuteron target

J. Yamagata-Sekihara[1,*], T. Sekihara[1], and D. Jido[2,3]

[1]*Institute of Particle and Nuclear Studies, High Energy Accelerator Research Organization (KEK), 1-1, Oho, Ibaraki 305-0801, Japan*
[2]*Yukawa Institute for Theoretical Physics, Kyoto University, Kyoto 606-8502, Japan*
[3]*J-PARC Branch, KEK Theory Center, Institute of Particle and Nuclear Studies, High Energy Accelerator Research Organization (KEK), 203-1, Shirakata, Tokai, Ibaraki, 319-1106, Japan*
*E-mail: yamajun@post.kek.jp

Received October 23, 2012; Accepted January 28, 2013; Published April 1, 2013

The $K^- d \to \pi Y N$ reaction is theoretically studied to investigate the K^--induced production of the hyperon resonances $\Sigma(1385)$ and $\Lambda(1405)$. For this purpose, we take into account the p-wave amplitudes for meson–baryon two-body scatterings as well as the s-wave amplitudes. Due to the fact that the hyperon resonances are selectively produced from the $\bar{K}N$ channel in this reaction, the $\Lambda(1405)$ peak appears at 1420 MeV, which implies that $\Lambda(1405)$ and $\Sigma(1385)$ could be separately seen in the missing-mass spectrum of the emitted nucleon in the $K^- d \to nX$ reaction. The πY invariant-mass spectrum in this study is consistent with experimental data both for $\Sigma(1385)$ and $\Lambda(1405)$. The pion exchange contributions are also included and are found to give a smooth background without distorting the peak structure of the hyperon resonances.

Subject Index D32

1. Introduction

The properties of hyperon resonances are important for understanding the role of strangeness in hadron physics. In particular, the understanding of hyperon resonances located below the $\bar{K}N$ threshold, such as $\Lambda(1405)$ and $\Sigma(1385)$, is essential for the physics of strangeness in nuclear matter and nuclei. In addition, because baryonic resonances decay into mesons and a baryon in strong interactions, one can learn about basic interactions between hadrons with strangeness from the properties of hyperon resonances.

Among the various hyperon resonances, recent attention is particularly focused on the $\Lambda(1405)$ hyperon resonance with $J^P = 1/2^-$ and $I = 0$. The $\Lambda(1405)$ resonance has long been considered a quasibound state of $\bar{K}N$ [1,2], being an extremely important resonance for understanding $\bar{K}N$ interaction. Theoretically, $\Lambda(1405)$ is successfully reproduced as dynamically generated states in the coupled-channel approach based on chiral dynamics [3–15], and this approach has confirmed that $\Lambda(1405)$ is predominantly described by meson–baryon components [16]. Recently, it has also been pointed out in Ref. [10] that $\Lambda(1405)$ is composed of two resonance states with different coupling natures and that the one that dominantly couples to the $\bar{K}N$ channel is located at 1420 MeV instead of nominal 1405 MeV. Since the resonance position of $\Lambda(1405)$ in the $\bar{K}N$ channel is strongly related to the strength of the $\bar{K}N$ interaction, it is very important to observe $\Lambda(1405)$ spectra in the $\bar{K}N \to \pi\Sigma$ channel and pin down the resonance position of $\Lambda(1405)$ seen below the $\bar{K}N$ threshold.

Several ideas for observing $\Lambda(1405)$ initiated by the $\bar{K}N$ channel have been proposed in Refs. [10, 17–24]. One of the promising ways of forming $\Lambda(1405)$ in the $\bar{K}N$ channel is to use nuclear reactions with a K^- beam, such as in-flight $K^-d \to \Lambda(1405)n$, as discussed in Refs. [21,22], in which the Fermi motion of the nucleon and $\bar{K}$ multi-scattering with nucleons help to create $\Lambda(1405)$ by $\bar{K}N$ below its threshold. In Ref. [21] it has been found that, in the $K^-d \to \Lambda(1405)n$ reaction with intermediate K^- beam energy, $\Lambda(1405)$ production dominantly takes place in a double scattering process, in which the incoming K^- kicks one of the nucleons in the deuteron in a forward direction, releasing its energy sufficiently to form $\Lambda(1405)$ with the other nucleon. Although a single scattering process also contributes to $\Lambda(1405)$ production, for energetic incoming K^- with several hundred MeV/c in the laboratory frame the contribution is small due to the insufficient Fermi motion of the nucleon in the deuteron. In addition, thanks to the fact that strangeness is brought into the system by the incoming K^-, $\Lambda(1405)$ is formed selectively by the $\bar{K}N$ channel[1]. This is a good advantage over $\Lambda(1405)$ production induced by a nonstrange particle, in which strangeness has to be created in the reaction process and can be carried by the baryon producing $\Lambda(1405)$. In fact, there is already an old bubble-chamber experiment observing $\Lambda(1405)$ in $K^-d \to \pi^+\Sigma^-n$ at K^- momenta between 686 and 844 MeV/c [25]. Although the statistics was not so high, the experiment clearly found that the $\Lambda(1405)$ spectrum has a peak at 1420 MeV. Forthcoming experiments in J-PARC with high-intensity kaon beams are expected to give more detailed and precise information on the properties of $\Lambda(1405)$ [26]. Recently, it has been pointed out in Ref. [27] that the method of determination of the kinematics in the loop given in Ref. [21] would break three-body unitarity. Later, in Ref. [23], the authors proposed several options for the kaon energy in the loop and found that the threshold effect does not affect the spectrum shape. In addition, since the $\Sigma(1385)$ resonance is far from the $\bar{K}N$ threshold, this issue is irrelevant for the $\Sigma(1385)$ resonance.

In this paper, we also apply this K^--induced production off a deuteron target to the $\Sigma(1385)$ resonance, which has $J^P = 3/2^+$ and $I = 1$ and is also located below the $\bar{K}N$ threshold. $\Sigma(1385)$ is well understood from the quark model point of view; it is classified as a flavor decuplet. Nevertheless, there are few theoretical discussions on $\Sigma(1385)$ formation in the $\bar{K}N$ channel. In addition, for precise determination of the $\Lambda(1405)$ properties from experiments, it is very important to understand the contributions of $\Sigma(1385)$ in the $\Lambda(1405)$ production process, because the $\Lambda(1405)$ and $\Sigma(1385)$ resonances are located at very similar energies, with widths of tens of MeV and overlapping spectra. This reaction also gives important information on the subthreshold production of $\Lambda(1405)$ and $\Sigma(1385)$, which will be significant in the strange few-body bound systems of $\bar{K}NN$ [28], $\bar{K}KN$ [29], and $\pi\Lambda N$ [30]. We also evaluate background contributions against $K^-d \to Y^*N$ by considering pion exchange contributions, in order to make a further comparison with the experimental spectra observed in Ref. [25].

This paper is organized as follows. In Sect. 2 we explain our scheme to calculate the production cross sections for $\Sigma(1385)$ as well as $\Lambda(1405)$. In Sect. 3 we show our numerical results of the calculations for the production cross sections. We also discuss non-resonant background contributions other than $\Sigma(1385)$ and $\Lambda(1405)$ to the mass spectra in this section. Section 4 is devoted to a summary of this study.

[1] Formation of $\Lambda(1405)$ by the $\pi\Sigma$ channel would take place by multi-pion exchange between two baryons. However, multi-pion exchange processes are absolutely negligible for the resonance formation with in-flight K^-.

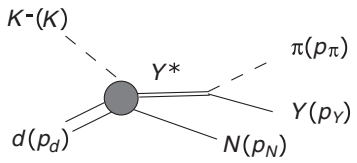

Fig. 1. Kinematics for the $K^- d \to \pi Y N$ reaction.

2. Formulation

In this study, we consider the $K^- d \to \pi^0 \Lambda n$, $(\pi\Sigma)^0 n$, $\pi^- \Lambda p$, and $(\pi\Sigma)^- p$ reactions so as to discuss the production of the hyperon resonances $\Sigma(1385)$ and $\Lambda(1405)$ initiated by the $\bar{K}N$ channel. The kinematical variables are given in Fig. 1. We discuss the kinematical aspects of the reactions in Sect. 2.1, followed by the dynamics of the reaction including the scattering amplitudes for the $K^- d$ reaction in Sect. 2.2 and the meson–baryon scattering amplitudes in the Appendix.

2.1. Reaction kinematics

The reaction $K^- d \to \pi Y N$ requires five variables to completely fix the phase-space of the three-body final state [31]. In this study we are interested in the mass spectra of the πY systems, thus we choose as the five variables the πY invariant mass $M_{\pi Y}$, the solid angle of the final N in the total center-of-mass frame Ω_N, and the solid angle of the final π in the πY center-of-mass Ω^*_π. Then, the cross section of the reaction is calculated by

$$d\sigma = \left(\frac{M_d M_Y M_N}{(2\pi)^4 4 k_{\text{c.m.}} E_{\text{c.m.}}} \right) |\mathcal{T}|^2 |\boldsymbol{p}_N| |\boldsymbol{p}^*_\pi| d M_{\pi Y} d\cos\theta_N d\Omega^*_\pi, \tag{1}$$

where M_d, M_Y, and M_N are the initial-state deuteron and final-state hyperon and nucleon masses in the reaction, respectively, $E_{\text{c.m.}}$ is the total center-of-mass energy, $k_{\text{c.m.}}$ is the K^- momentum in the total center-of-mass frame, θ_N is the scattering angle of N with respect to K^- in the total center-of-mass frame, and $\mathcal{T}$ is the T-matrix of the reaction. In this form the azimuthal angle of Ω_N is integrated.

Now let us pin down the reaction mechanism. Since we want to produce hyperon resonances in the final state, diagrams in which π and Y come from the same vertices are essential. Here, following Ref. [21], we evaluate the impulse and double scattering amplitudes for the production of the hyperon resonances.

First, we consider the $K^- d$ reaction with neutron emission in the final state. The relevant diagrams for this reaction are given in Fig. 2. Diagram 1 in Fig. 2 corresponds to the impulse process for hyperon resonance production, whereas diagrams 2 and 3 are double scattering processes. We emphasize that the conservation of strangeness in the strong interaction guarantees the production of hyperon resonances from the $\bar{K}N$ channel both in the impulse and double scattering processes. The πY systems are fixed as charge zero ones, $\pi^0\Lambda$, $\pi^+\Sigma^-$, $\pi^-\Sigma^+$, and $\pi^0\Sigma^0$. The $\pi^0\Lambda$ ($\pi^0\Sigma^0$) mass spectrum will be dominated by $\Sigma(1385)$ ($\Lambda(1405)$), since it is a purely $I = 1$ (0) channel. The $\pi^+\Sigma^-$ and $\pi^-\Sigma^+$ mass spectra can contain $\Sigma(1385)$ in addition to $\Lambda(1405)$, since $\Sigma(1385)$ has a branching ratio of 12% to the $\pi\Sigma$ channel.

Second, we consider the $K^- d$ reaction with proton emission in the final state. The relevant diagrams are given in Fig. 3. In this case we have only two diagrams so as to emit the final-state π and Y from the same vertex; one is the impulse diagram and the other the double scattering diagram. The

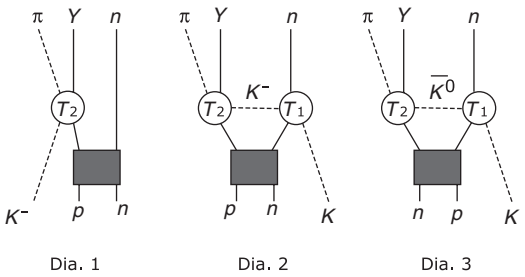

Fig. 2. Diagrams for the $K^- d \to \pi Y n$ reaction. In the diagrams, T_1 and T_2 denote the scattering amplitudes for $K^- N \to \bar{K} n$ and $\bar{K} N \to \pi Y$, respectively.

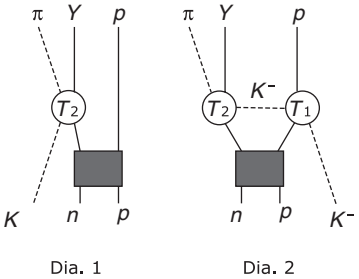

Fig. 3. Diagrams for the $K^- d \to \pi Y p$ reaction. In the diagrams, T_1 and T_2 denote the scattering amplitudes for $K^- p \to K^- p$ and $K^- n \to \pi Y$, respectively.

πY systems are $\pi^- \Lambda$, $\pi^- \Sigma^0$, and $\pi^0 \Sigma^-$, and all of them contain only the $\Sigma^-(1385)$ contribution as hyperon resonances of interest.

Now that we have determined the reaction diagrams, all we have to do is the evaluation of the scattering amplitudes, which contain the dynamics of the hyperon resonance production.

2.2. $K^- d$ scattering amplitudes

In this section, we formulate the scattering amplitudes of the $K^- d$ reaction given in Figs 2 and 3. These amplitudes are composed of $\bar{K} N \to \bar{K} N$ and πY amplitudes, a kaon propagator, and a deuteron wave function. We study both $\Sigma(1385)$ and $\Lambda(1405)$ in the reaction by including s- and p-wave contributions in the $\bar{K} N$ amplitudes. It is important that the p-wave contribution requires a nucleon spin component in the deuteron wave function, which is not needed in the case of $\Lambda(1405)$ production with the s-wave $\bar{K} N$ amplitudes [21].

First, we formulate the amplitude of the impulse approximation given in Figs 2(1) and 3(1). According to Ref. [21] and taking into account the spin component inside the deuteron, we can write the scattering amplitude for the impulse approximation as

$$\mathcal{T}^a_{\pi Y n(1)} = T_{K^- p \to \pi Y}(M_{\pi Y}, \hat{p_\pi} \cdot \hat{k})(S^\dagger)^a \tilde{\varphi}\left(\left|\boldsymbol{p}_n - \frac{\boldsymbol{p}_d}{2}\right|\right), \tag{2}$$

$$\mathcal{T}^a_{\pi Y p(1)} = T_{K^- n \to \pi Y}(M_{\pi Y}, \hat{p_\pi} \cdot \hat{k})(S^\dagger)^a \tilde{\varphi}\left(\left|\boldsymbol{p}_p - \frac{\boldsymbol{p}_d}{2}\right|\right). \tag{3}$$

Here, $T_{\bar{K} N \to M B}$ is the $\bar{K} N \to M B$ amplitude in a 2×2 matrix form, which compensates the Pauli spinor for baryons, and is a function of the center-of-mass energy $M_{\pi Y}$ and the angle $\hat{k} \cdot \hat{p}_\pi$ in the meson–baryon center-of-mass frame, $(S^\dagger)^a = -i\sigma^2\sigma^a/\sqrt{2}$ $(a = 1, 2, 3)$ is the spinor component for each nucleon inside the deuteron in a 2×2 matrix form, and $\tilde{\varphi}(p)$ is the momentum representation of the deuteron wave function with momentum p, for which we neglect the d-wave component

and use a parameterization of the s-wave component given by an analytic function [32] as

$$\tilde{\varphi}(p) = \sum_{j=1}^{11} \frac{C_j}{p^2 + m_j^2}, \tag{4}$$

with C_j and m_j determined in Ref. [33].

Second, let us consider the double scattering amplitudes. According to Ref. [21] and taking into account the spin component inside the deuteron, the double scattering amplitudes are formulated as

$$\begin{aligned}\mathcal{T}^a_{\pi Yn(2)} = &\int \frac{d^3q}{(2\pi)^3} T_{K^-p\to\pi Y}(M_{\pi Y}, \hat{q}\cdot\hat{p_\pi})(S^\dagger)^a T^t_{K^-n\to K^-n}(W, \hat{k}\cdot\hat{q}) \\ &\times \frac{\tilde{\varphi}(|\boldsymbol{q} + \boldsymbol{p}_n - \boldsymbol{k} - \boldsymbol{p}_d/2|)}{q^2 - m^2_{K^-} + i\epsilon},\end{aligned} \tag{5}$$

$$\begin{aligned}\mathcal{T}^a_{\pi Yn(3)} = &-\int \frac{d^3q}{(2\pi)^3} T_{\bar{K}^0n\to\pi Y}(M_{\pi Y}, \hat{q}\cdot\hat{p}_\pi)(S^\dagger)^a T^t_{K^-p\to\bar{K}^0n}(W, \hat{k}\cdot\hat{q}) \\ &\times \frac{\tilde{\varphi}(|\boldsymbol{q} + \boldsymbol{p}_n - \boldsymbol{k} - \boldsymbol{p}_d/2|)}{q^2 - m^2_{\bar{K}^0} + i\epsilon},\end{aligned} \tag{6}$$

$$\begin{aligned}\mathcal{T}^a_{\pi Yp(2)} = &\int \frac{d^3q}{(2\pi)^3} T_{K^-n\to\pi Y}(M_{\pi Y}, \hat{q}\cdot\hat{p}_\pi)(S^\dagger)^a T^t_{K^-p\to K^-p}(W, \hat{k}\cdot\hat{q}) \\ &\times \frac{\tilde{\varphi}(|\boldsymbol{q} + \boldsymbol{p}_p - \boldsymbol{k} - \boldsymbol{p}_d/2|)}{q^2 - m^2_{K^-} + i\epsilon},\end{aligned} \tag{7}$$

where q^0 and W are fixed as $q^0 = k^0 + M_1 - p^0_N$ and $W = \sqrt{(M_1 + k^0)^2 - \boldsymbol{k}^2}$, with M_1 the first-scattered nucleon mass and p^0_N the energy of the final-state nucleon. This prescription of q^0 takes account of the NN potential in the deuteron nonperturbatively, as suggested in the Watson formulation [23]. The superscript t denotes the transposition of the matrix in the spin space.

In our approach, the $\bar{K}N \to \bar{K}N$ and πY amplitudes are essential to the production of the hyperon resonances. For the meson–baryon amplitudes we apply the so-called chiral unitary approach [3–10]. In the chiral unitary approach, $\Lambda(1405)$ is dynamically generated by the unitarized coupled-channel method based on chiral dynamics without explicit poles [16]. In contrast, $\Sigma(1385)$ can be included as an explicit pole in the p-wave kernel interactions in the coupled-channel approach [34]. The details of the description of the $\bar{K}N \to \bar{K}N$ and πY amplitudes for $\Lambda(1405)$ and $\Sigma(1385)$ are given in Appendix A.

The chiral unitary amplitude has been calculated in the center-of-mass frame of the two-body meson–baryon system. Since the deuteron wave function has been calculated in the rest frame of the deuteron, we calculate the $K^-d \to \pi YN$ amplitude in the laboratory frame, in which the target deuteron is at rest. Thus, we make a transformation of the amplitude obtained in the two-body center-of-mass frame to the baryon rest frame using the method shown in Appendix B. For the p-wave amplitude, we define the off-shell behavior by using a form factor

$$f_\Lambda(|\boldsymbol{q}|) = \frac{\Lambda^2}{\Lambda^2 + \boldsymbol{q}^2}, \tag{8}$$

with $\Lambda = 630\,\text{MeV}$, which has been used in the chiral unitary model for the s-wave.

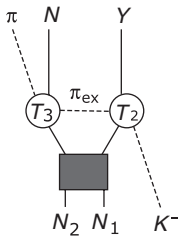

Fig. 4. Diagrams of the π meson exchange contribution. T_2 and T_3 denote the scattering amplitudes for $\bar{K}N \to \pi Y$ and $\pi N \to \pi N$, respectively.

Table 1. Possible exchange pions for the diagram shown in Fig. 4.

Reaction	N_1	N_2	$\pi_{\rm ex}$
$K^- d \to \pi^+ \Sigma^- n$	p	n	π^+
	n	p	π^0
$K^- d \to \pi^- \Sigma^+ n$	p	n	π^-
$K^- d \to \pi^0 \Sigma^0 n$	n	p	π^-
	p	n	π^0
$K^- d \to \pi^0 \Lambda n$	n	p	π^-
	p	n	π^0
$K^- d \to \pi^- \Lambda p$	n	p	π^-
	p	n	π^0

The total amplitude for $K^- d \to \pi Y n$ and $\pi Y p$ is given by the coherent sum of the impulse and double scattering contributions as

$$\mathcal{T}^a_{\pi Y n} = \mathcal{T}^a_{\pi Y n(1)} + \mathcal{T}^a_{\pi Y n(2)} + \mathcal{T}^a_{\pi Y n(3)}, \tag{9}$$

$$\mathcal{T}^a_{\pi Y p} = \mathcal{T}^a_{\pi Y p(1)} + \mathcal{T}^a_{\pi Y p(2)}, \tag{10}$$

respectively. Then, the squared amplitude spin-summed for the final state and averaged in the initial state (deuteron) is given as

$$|\mathcal{T}|^2 = \frac{1}{3}\sum_{a=1}^{3} \mathrm{tr}[\mathcal{T}^a (\mathcal{T}^a)^\dagger], \tag{11}$$

denoting the trace of the 2×2 spin space matrix by "tr".

2.3. Estimation of the pion exchange contributions

It is instructive to estimate the pion exchange contribution to the production of the hyperon resonances, which mainly comes from the amplitudes without πY correlation in the final state. In the estimation of the pion exchange amplitude, we evaluate the diagrams given in Fig. 4. The particles, which are correlated with the pion exchange process, are listed in Table 1. They contain the $\pi N \to \pi N$ amplitude, which does not appear in the usual diagrams for the production of hyperon resonances given in Figs 2 and 3. For the $\pi N \to \pi N$ amplitude, we take an empirical amplitude [35] up to the p-wave including the $\Delta(1232)$ resonance, which is obtained based on the observed scattering data. The off-shell extrapolation is done in the same way for the kaon exchange. We show a Dalitz plot in order to see the energy range of the πN amplitude. In Fig. 5, we have found that the πN energy range, which is considered from $\Lambda(1405)$ and $\Sigma(1385)$ production, includes $\Delta(1232)$ resonance. Therefore, the contribution of $\Delta(1232)$ production seems to be mainly smooth background from πN scattering in $\Lambda(1405)$ and $\Sigma(1385)$ production.

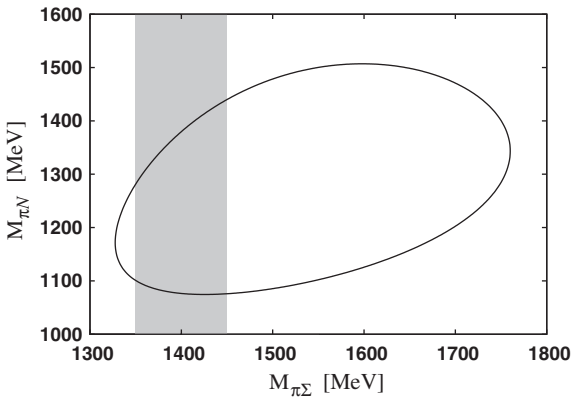

Fig. 5. Dalitz plot for the $\pi^0\Sigma^0 n$ final state with 800 MeV/c incident K^- momenta. The masked area shows the πY energy range (1350–1450 MeV) considered in this work.

3. Numerical results

In this section we show our numerical results for the production of hyperon resonances $\Sigma(1385)$ and $\Lambda(1405)$ in the $K^- d$ reactions. Using Eq. (1), we can evaluate the differential cross section as

$$\frac{d^2\sigma}{dM_{\pi Y} d\cos\theta_N} = \frac{M_d M_Y M_N}{(2\pi)^4 4k_{\text{c.m.}} E_{\text{c.m.}}} |\boldsymbol{p}_N||\boldsymbol{p}_\pi^*| \int d\Omega_\pi^* |\mathcal{T}|^2, \tag{12}$$

with the $K^- d \to \pi Y N$ scattering amplitude $\mathcal{T}$, which includes the pion exchange process. Then, integrating $\cos\theta_N$, one can obtain the πY mass spectrum:

$$\frac{d\sigma}{dM_{\pi Y}} = \frac{M_d M_Y M_N}{(2\pi)^4 4k_{\text{c.m.}} E_{\text{c.m.}}} |\boldsymbol{p}_N||\boldsymbol{p}_\pi^*| \int_{-1}^{1} d\cos\theta_N \int d\Omega_\pi^* |\mathcal{T}|^2. \tag{13}$$

Further, integrating $M_{\pi Y}$ with an appropriate range (M_{min}, M_{max}) for the hyperon resonances, the production cross section for the hyperon resonances is obtained as

$$\sigma = \frac{M_d M_Y M_N}{(2\pi)^4 4k_{\text{c.m.}} E_{\text{c.m.}}} \int_{M_{\text{min}}}^{M_{\text{max}}} dM_{\pi Y} |\boldsymbol{p}_N||\boldsymbol{p}_\pi^*| \int_{-1}^{1} d\cos\theta_N \int d\Omega_\pi^* |\mathcal{T}|^2. \tag{14}$$

It is also interesting to calculate the angular dependence of the production by

$$\frac{d\sigma}{d\cos\theta_N} = \frac{M_d M_Y M_N}{(2\pi)^4 4k_{\text{c.m.}} E_{\text{c.m.}}} \int_{M_{\text{min}}}^{M_{\text{max}}} dM_{\pi Y} |\boldsymbol{p}_N||\boldsymbol{p}_\pi^*| \int d\Omega_\pi^* |\mathcal{T}|^2. \tag{15}$$

In this study, we evaluate the $K^- d$ amplitudes in Figs 2 and 3 by using the chiral unitary approach for the description of the meson–baryon scattering amplitudes. In this approach, $\Lambda(1405)$ is dynamically generated without introducing explicit poles in the s-wave amplitude, whereas $\Sigma(1385)$ is included as an explicit pole in the p-wave amplitude.

First, we compare our results with experiments in Sect. 3.1. Next, in Sect. 3.2, theoretical studies of the production of the hyperon resonances are given.

3.1. Production of hyperon resonances: Comparison with experimental data

3.1.1. $\Sigma(1385)$ production. First of all, we show the results of the $\Sigma(1385)$ production and make a comparison with the experimental data [25]. For the $\Sigma(1385)$ production, it is better to see the $K^- d \to \pi^- \Lambda p$ reaction, in which $\Lambda(1405)$ does not contribute to the $\pi^-\Lambda$ mass spectrum. Here, we include the pion exchange contribution in addition to the kaon exchange contribution for the hyperon resonance production.

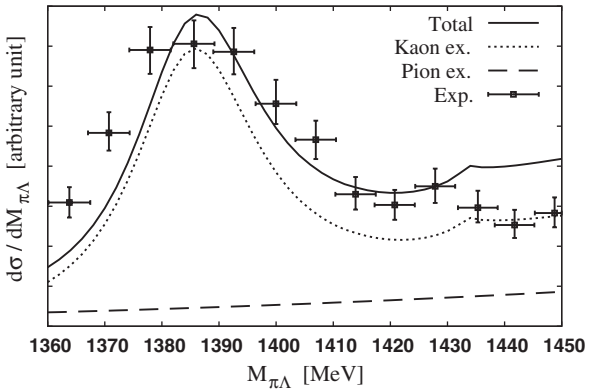

Fig. 6. $\pi^-\Lambda$ invariant-mass spectrum of the $K^-d \to \pi^-\Lambda p$ reaction in arbitrary units at 800 MeV/c incident K^- momentum. The solid line denotes the present calculation, and the dotted line and dashed line are the contributions from kaon exchange and pion exchange, respectively. Experimental data are taken from Ref. [25] at K^- momenta between 686 MeV/c and 844 MeV/c.

Using Eq. (13), we show the $\pi^-\Lambda$ mass spectrum in the $K^-d \to \pi^-\Lambda p$ reaction in Fig. 6, together with the experimental data [25], which includes the background contribution. Here, the kaon momentum is fixed at 800 MeV/c in our calculation, whereas the range of the initiated kaon momentum is from 686 to 844 MeV/c in the experiment [25]. As seen in the figure, we can well reproduce the experimental mass spectrum with the $\Sigma(1385)$ peak around 1385 MeV of the $\pi^-\Lambda$ invariant mass.

Next, let us evaluate the cross section of the $\Sigma(1385)$ production. In principle, such cross sections for the resonances can be evaluated theoretically by taking the residue of the scattering amplitude at the resonance pole. Here we use a more phenomenological technique for the comparison with experimental data, as follows. Since the pion exchange contribution gives only the non-resonant background, we take only the kaon exchange contribution for the production cross section, and integrate it in the range of $M_{\rm min} = 1370$ MeV and $M_{\rm max} = 1400$ MeV:

$$\sigma_{\Sigma^*} = \frac{1}{0.88}\int_{M_{\rm min}}^{M_{\rm max}} dM_{\pi^-\Lambda}\frac{d\sigma_{\rm F.G}}{dM_{\pi^-\Lambda}}, \tag{16}$$

where factor $1/0.88$ comes from the branching ratio of $\Sigma(1385) \to \pi\Lambda$, 88%, and $\sigma_{\rm F.G.}$ is the cross section by the foreground process (kaon exchange contribution). We obtain the $\Sigma(1385)$ production cross section as 179 μb with 800 MeV/c incident K^-, whereas the experimental value observed in the $K^-d \to \pi^-\Lambda p$ reaction is reported to be 252 ± 30 μb at 778 MeV/c of the incident K^- momentum [25]. As one can see, our cross section is consistent with the experimental value. There is, however, a small difference between our theoretical production cross section and the experimental one. This difference may come from the ways of subtracting the background contribution of the resonance. In Ref. [25], the background contributions have been estimated by fitting the mass spectrum in a sum of Legendre polynomials together with a relativistic Breit–Wigner form for the resonance. In the theoretical side, we have estimated the production cross section by using the diagrams in which π^- and Λ are emitted from the same vertex and we have not subtracted the non-resonant background appearing in the $K^-n \to \pi^-\Lambda$ amplitude from $\Sigma(1385)$, which is clearly seen above the 1400 MeV of the invariant mass $\pi^-\Lambda$. We also note that the value of the production cross section depends on the choice of the range of the invariant-mass integration.

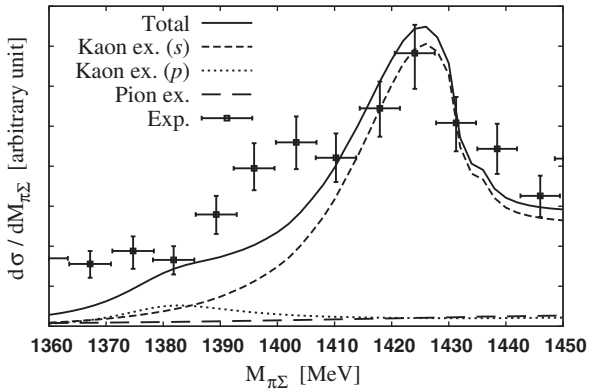

Fig. 7. $\pi^+\Sigma^-$ invariant-mass spectrum of the $K^-d \to \pi^+\Sigma^- n$ reaction in arbitrary units at 800 MeV/c incident K^- momentum. The solid line denotes the result of the full calculation with both s- and p-wave contributions, whereas the dashed (dotted) line denotes the contribution from the kaon exchange s- (p-) wave component in the $\bar{K}N \to \pi^+\Sigma^-$ amplitude. The dashed line corresponds to the result in Ref. [21]. The long–dashed line denotes the pion exchange contribution. Experimental data are taken from Ref. [25] at K^- momenta between 686 MeV/c and 844 MeV/c.

Finally, we should note that above the 1420 MeV of the $\pi^-\Lambda$ invariant mass, the mass spectrum is not suppressed, although this is far above the $\Sigma(1385)$ energy region. This comes from the $I = 1$ non-resonant background in the $\bar{K}N$ scattering, which can interfere with $\Lambda(1405)$.

3.1.2. $\Lambda(1405)$ *production.* Next we show the results of $\Lambda(1405)$ production in the K^-d reaction. For $\Lambda(1405)$ production we choose the $K^-d \to \pi^+\Sigma^- n$ reaction and calculate the $\pi^+\Sigma^-$ mass spectrum. Here we note that the $\pi^+\Sigma^-$ spectrum comes not only from $\Lambda(1405)$ but also from $\Sigma^0(1385)$, whose branching ratio to $\pi\Sigma$ is about 12%.

First, we show the $\pi^+\Sigma^-$ mass spectrum of the $K^-d \to \pi^+\Sigma^- n$ reaction in Fig. 7, together with the experimental data [25]. In the previous paper [21], the K^-d reaction with only the s-wave meson–baryon amplitude was calculated, whereas in this study we include both s- and p-wave meson–baryon amplitudes. In Fig. 7, we plot the full calculation with a coherent sum of s- and p-wave contributions with the solid line, whereas the s- (p-) wave contribution to the $\bar{K}N \to \pi^+\Sigma^-$ amplitude (T_2 in Figs 2 and 3) is shown by the dashed (dotted) line. The $K^-N \to \bar{K}N$ amplitudes T_1 in Figs 2 and 3 are fixed to be a coherent sum of the s- and p-wave contributions in every case. As can be seen from the figure, we reproduce well the experimentally observed mass spectrum of the reaction. We can see that the $\Lambda(1405)$ peak appears at 1420 MeV in $\pi^+\Sigma^-$ invariant mass instead of nominal 1405 MeV as in Ref. [21], without contamination from $\Sigma(1385)$ or the p-wave background contribution. Furthermore, it is important that the $\Sigma(1385)$ contribution appears as a shoulder around 1390 MeV $\pi^+\Sigma^-$ invariant mass, which may explain the bump structure in the empirical data.

Next, let us consider the $\Lambda(1405)$ production cross section from the kaon exchange contribution, which is calculated by the formula

$$\sigma_{\Lambda^*} = 3\int_{M_{\rm min}}^{M_{\rm max}} dM_{\pi^+\Sigma^-}\frac{d\sigma_{\rm F.G}}{dM_{\pi^+\Sigma^-}} \tag{17}$$

with the range $M_{\rm min} = 1400$ MeV and $M_{\rm max} = 1440$ MeV. The factor 3 comes from the branching ratio of $\Lambda(1405) \to \pi^+\Sigma^-$, 33%. The $\Lambda(1405)$ production cross section is consistent with the empirical value [25], as obtained previously in Ref. [21].

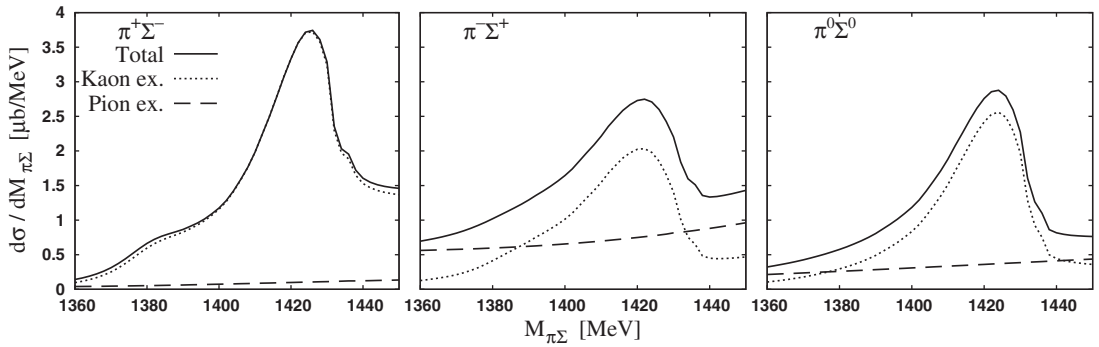

Fig. 8. $\pi\Sigma$ invariant-mass spectrum for different $\pi\Sigma$ states at 800 MeV/c incident K^- momentum.

3.2. *Production of hyperon resonances: Theoretical studies*

For the understanding of the production of the hyperon resonances in the K^-d reaction, it is important to investigate theoretically the production mechanism of the reaction. Therefore, we undertake theoretical studies of the K^-d reaction in this subsection.

3.2.1. $\pi\Sigma$ channel components. For clarification of the $\Lambda(1405)$ properties, it is important to understand the behavior of each $\pi\Sigma$ channel spectrum. Hence, we plot the $\pi^+\Sigma^-$, $\pi^-\Sigma^+$, and $\pi^0\Sigma^0$ mass spectra in the $K^-d \to (\pi\Sigma)^0 n$ reaction in Fig. 8. Here the initial kaon momentum is fixed at 800 MeV/c.

From Fig. 8, one can see that the behavior of the $\pi\Sigma$ mass spectra differs slightly between the spectra. This is due to the interference between the $\Lambda(1405)$ contribution ($I = 0$) and the $I = 1$ non-resonant contribution. The significant non-resonant contribution with $I = 1$ around the $\Lambda(1405)$ energy can be seen in the $\pi^-\Lambda$ spectrum shown in Fig. 6. As a consequence of the interference, the $\pi^+\Sigma^-$ spectrum shows the largest contribution of $\Lambda(1405)$ production and has a peak position at a higher energy than the $\pi^-\Sigma^+$ spectrum, which is consistent with the results obtained in Ref. [21]. The interference between the $\Lambda(1405)$ and $I = 1$ contributions has been, indeed, important in the photoproduction of $\Lambda(1405)$ [36–38]. Therefore, experimental data on the $\pi^\pm\Sigma^\mp$ spectrum will bring us further information on the $\Lambda(1405)$ structure.

We also note that the $\pi^0\Sigma^0$ spectrum does not show the $\Sigma(1385)$ contribution, because the $\pi^0\Sigma^0$ channel does not contain an $I = 1$ component. Hence, it will be important to observe all three $(\pi\Sigma)^0$ spectra in the K^-d reaction and compare them in the experiment to obtain understanding of the $\Lambda(1405)$ structure.

3.2.2. Diagram contributions. For the understanding of the K^-d reaction, it is helpful to investigate each diagram contribution to the production of hyperon resonances. Here we show the $\pi^0\Sigma^0$ and $\pi^0\Lambda$ invariant-mass spectra separately plotted in each diagram contribution in Fig. 9. The incident kaon momentum is 800 MeV/c.

As can be seen, both $\Lambda(1405)$ in the $\pi^0\Sigma^0$ spectrum and $\Sigma(1385)$ in the $\pi^0\Lambda$ spectrum show that diagram 1 (impulse contribution) in the reaction (Fig. 2) makes quite a small contribution, whereas diagram 2 in the reaction (Fig. 2) has the largest contribution. The reason that diagram 1, corresponding to the impulse production of the hyperon resonances, makes a small contribution is that the nucleons inside the deuteron hardly have higher momentum component as discussed in Ref. [21]. Namely, in order to produce the hyperon resonances below the $\bar{K}N$ threshold, one needs to create

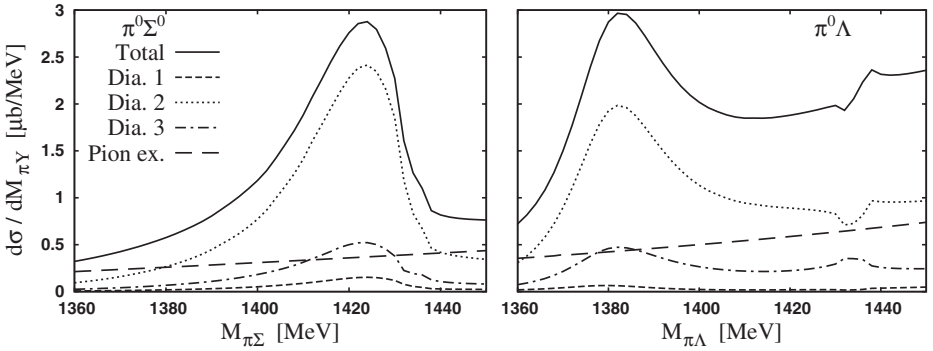

Fig. 9. $\pi^0\Sigma^0$ (left panel) and $\pi^0\Lambda$ (right panel) invariant-mass spectra separately plotted in each diagram contribution. The incident K^- momentum is 800 MeV/c. The solid line shows the kaon exchange contributions of three diagrams and the pion exchange diagrams. The dashed, dotted, and dash-dotted lines show the contributions from diagrams 1, 2, and 3 as shown in Fig. 2, respectively. The long-dashed line shows the pion exchange contribution.

an energetic nucleon in the final state of the $K^-d \to \pi YN$ reaction. Such an energetic nucleon is, however, scarcely produced in the impulse process of the K^-d reaction, because the large Fermi momentum of the nucleon is highly suppressed by the deuteron wave function due to the small binding energy. As a consequence, the impulse production of the hyperon resonances makes quite a small contribution.

Compared with the impulse process, the double scattering process (diagrams 2 and 3) is kinematically favored. Namely, in the double scattering process, the transferred energy can be taken from the incident kaon so that the exchanged kaon has less energy than that on-shell, which is favorable for the production of hyperon resonances below the $\bar{K}N$ threshold. Among the double scattering, since the $K^-n \to K^-n$ amplitude takes a larger value than that of the $K^-p \to \bar{K}^0n$ amplitude in the energy region considered, diagram 2 makes the largest contribution to both $\Lambda(1405)$ and $\Sigma(1385)$ production (see also the discussion in Ref. [21]).

3.2.3. Angular dependence of production. Now let us see the angular dependence of the production of the hyperon resonances. First of all, we show the double-differential cross section $d^2\sigma/dM_{\pi\Sigma}d\cos\theta_n$ in the $K^-d \to \pi^+\Sigma^-n$ reaction in Fig. 10, in which the incident kaon momentum is fixed to be 800 MeV/c. In this reaction we can see the two peaks coming from two resonances, $\Sigma(1385)$ around 1385 MeV and $\Lambda(1405)$ around 1420 MeV, for $60^\circ \le \theta_n \le 150^\circ$.

As one can see, the $\Lambda(1405)$ peak has strong angular θ_n dependence. The $\Lambda(1405)$ peak takes its largest value at $\theta_n = 0^\circ$, which corresponds to the forward neutron emission in the total center-of-mass frame, and it becomes about 10 times smaller in the region $\theta_n \ge 60^\circ$. The reason for this is as follows. The momentum transfer by the exchanged kaon becomes smaller in the double scattering process in the region $\theta_n \le 60^\circ$, because in this case the incident kaon kicks out a neutron in the direction of the incident kaon and simply gives most of its momentum to the neutron in the first double scattering step. This small momentum transfer makes the exchanged kaon close to being on the mass shell, in which the double scattering amplitude takes a larger value. Hence, due to the kinematical reasons of dominant double scattering (discussed in the previous section) and of suitable momentum transfer, the $\Lambda(1405)$ peak has a large angular dependence and consequently backward $\Lambda(1405)$ production is dominant.

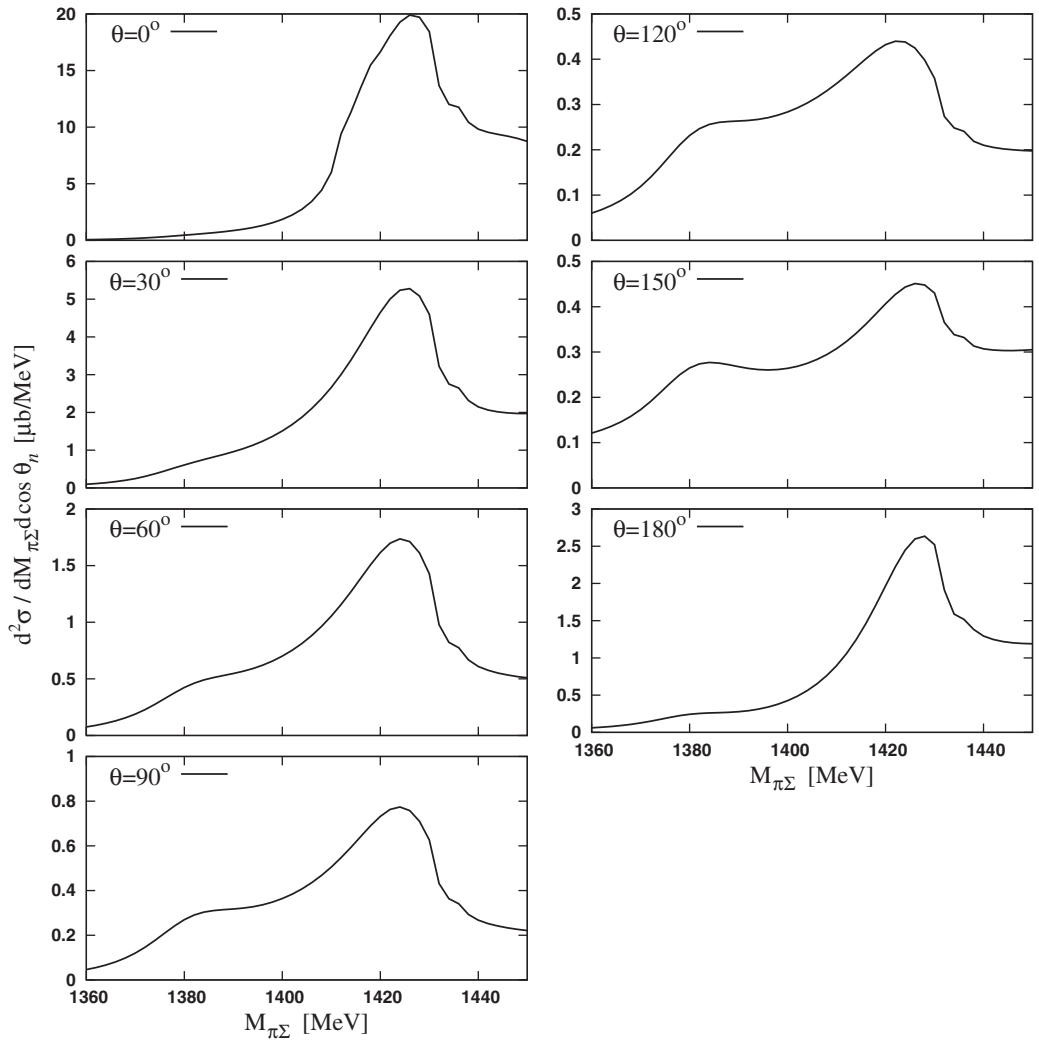

Fig. 10. Angular dependence of the $\pi^+\Sigma^-$ invariant-mass spectrum at 800 MeV/c incident K^- momentum. The values of θ in the figure are given in units of degrees.

The $\Sigma(1385)$ peak, on the other hand, shows only small angular dependence in the $K^-d \to \pi^+\Sigma^- n$ reaction. This is caused by the p-wave nature of $\Sigma(1385)$ in meson–baryon scattering. Namely, since the p-wave amplitude depends linearly on the transferred momentum, $\Sigma(1385)$ cannot be greatly produced with the neutron forward angle, in which the momentum transfer becomes smaller (as discussed above). This momentum transfer becomes larger as the angle θ_n becomes larger, since the incident kaon has to kick out a neutron in the opposite direction of the kaon momentum in the first double scattering step. Therefore, as a combination of the p-wave nature of $\Sigma(1385)$ and a suitable region for momentum transfer in the process, $\Sigma(1385)$ production shows small angular dependence although, in the middle θ_n region, the production is not favored by the kinematics.

The angular dependence of the hyperon resonance production is clearly seen in the differential cross section $d\sigma/d\cos\theta_n$ with the integration range ($M_{\min}$, $M_{\max}$) given in Sect. 3.1. In Fig. 11, we plot $d\sigma/d\cos\theta_n$ for $\Lambda(1405)$ ($\Sigma(1385)$) production in the $K^-d \to \pi^0\Sigma^0 n$ ($\pi^0\Lambda n$) reaction. From Fig. 11, we can see that $\Lambda(1405)$ is produced dominantly in the forward neutron angle, whereas the $\Sigma(1385)$ production moderately depends on the neutron angle.

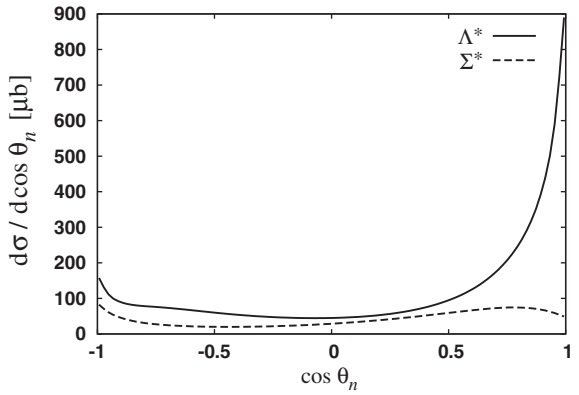

Fig. 11. Angular dependence of the $\Lambda(1405)$ and $\Sigma^0(1385)$ production cross sections in the $K^- d \to \pi^0 \Sigma^0 n$ (for $\Lambda(1405)$) and $\pi^0 \Lambda n$ (for $\Sigma^0(1385)$) reactions.

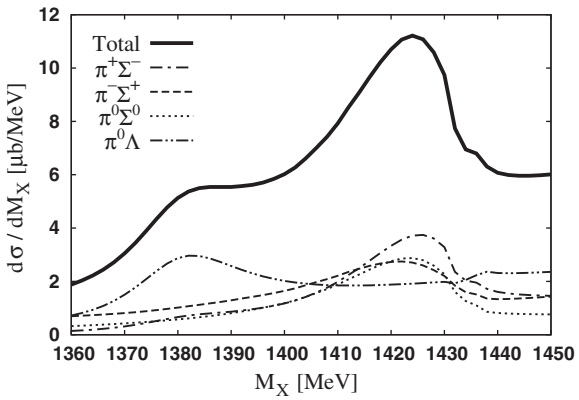

Fig. 12. Missing-mass spectrum in the $K^- d \to nX$ process at 800 MeV/c incident K^- momentum. The solid, dashed, dashed-dotted, and dashed-double-dotted lines are the total, $\pi^- \Sigma^+$, $\pi^0 \Sigma^0$, $\pi^+ \Sigma^-$, and $\pi^0 \Lambda$ contributions to X.

3.2.4. Missing-mass spectrum. As we have seen in the previous sections, the $\Lambda(1405)$ peak appears at 1420 MeV instead of nominal 1405 MeV in the $\pi\Sigma$ invariant mass of the $K^- d \to \pi \Sigma n$ reaction, thanks to the selective $\Lambda(1405)$ production by the $\bar{K}N$ channel. This fact implies that there is a possibility that the $\Sigma(1385)$ and $\Lambda(1405)$ peaks are seen separately in the $\pi\Sigma$ mass spectrum of the $K^- d$ reaction; they are usually mixed together due to their similar peak energies. Here, in order to investigate the behavior of the peak structures, we plot the missing-mass spectrum of the reaction $K^- d \to nX$. In the energy region around 1400 MeV, the missing-mass spectrum is expected to be dominated by the $(\pi Y)^0$ system. Hence, evaluating the relevant diagrams shown in Figs 2 and 3 and neglecting the amplitudes in which π and Y do not correlate with each other, which will give no structure in the missing-mass spectrum, we can plot the missing-mass spectrum in Fig. 12. As one can see, a double-peak structure appears, coming from $\Sigma(1385)$ (around 1385 MeV) and $\Lambda(1405)$ (around 1420 MeV). In the missing-mass spectrum, the $\Sigma(1385)$ peak comes from the $\pi^0 \Lambda$ and the $\Lambda(1405)$ peak from the $(\pi\Sigma)^0$ channel. The reason why we can separate the $\Sigma(1385)$ peak and the $\Lambda(1405)$ one is, as discussed above, because we can produce $\Lambda(1405)$ from the $\bar{K}N$ initial channel, pinning down the production process via conservation of strangeness.

4. Summary

We have undertaken a study of the $\Sigma(1385)$ and $\Lambda(1405)$ production induced by K^- on a deuteron target by calculating the $K^-d \to \pi Y N$ reaction. We have taken into account both the s- and p-wave contributions of meson–baryon scattering in the K^-d reaction; in particular, the contribution of the $\Sigma(1385)$ resonance is newly considered in this study. In the $K^-d \to \pi Y N$ reaction, the hyperon resonances are created selectively by the $\bar{K}N$ channel. Thanks to this fact, the higher pole state of $\Lambda(1405)$ is produced and the $\pi\Sigma$ spectrum has a peak at around 1420 MeV. This finding implies that $\Lambda(1405)$ and $\Sigma(1385)$ could be seen separately in the missing-mass spectrum of the emitted nucleon in the $K^-d \to nX$ reaction. We have found that the invariant-mass spectrum of πY is consistent with experimental data [25], both for the $\Sigma(1385)$ and $\Lambda(1405)$ cases. We have investigated the angular dependence of the hyperon resonances and found that $\Lambda(1405)$ production mainly takes place in the backward direction, while $\Sigma(1385)$ production does not strongly depend on the angle of the emitted nucleon. We studied the production mechanisms of $\Sigma(1385)$ and $\Lambda(1405)$ from the theoretical side. We have also estimated the pion exchange contributions coming from diagrams in which π and Y are not correlated with each other and found that these contributions give a smooth background and do not spoil the peak structure of the hyperon resonances.

Acknowledgements

This work was supported in part by a Grant-in-Aid for Scientific Research from MEXT and JSPS (Nos. 22740161, 24105706), a collaboration agreement between the JSPS of Japan and the CSIC of Spain, and a Grant-in-Aid for the Global COE Program "The Next Generation of Physics, Spun from Universality and Emergence" from MEXT of Japan. This work is partly supported by DGICYT contract number FIS2006-03438. We acknowledge the support of the European Community Research Infrastructure Integrating Activity "Study of Strongly Interacting Matter" (acronym HadronPhysics2, Grant Agreement n. 227431) under the Seventh Framework Programme of the EU. This work is part of the Yukawa International Program for Quark–Hadron Sciences (YIPQS).

Appendix A. Chiral unitary model for $\Lambda(1405)$ and $\Sigma(1385)$

Let us briefly formulate the meson–baryon scattering amplitude in the chiral unitary approach. First of all, in order to include the higher orbital angular momenta for the meson–baryon system, we expand the amplitude $T_{ji}(W, x)$ (i and j denote the initial and final meson–baryon channels, respectively, W the center-of-mass energy, and $x = \cos\theta$ with the scattering angle θ in the center-of-mass frame) into the partial wave as

$$T_{ji}(W, x) = F_{ji}(W, x)\delta_{s_j s_i} - iG_{ji}(W, x)(\hat{k}' \times \hat{k}) \cdot \boldsymbol{\sigma}_{s_j s_i}, \tag{A1}$$

$$F_{ji}(W, x) = \sum_{l=0}^{\infty} \left[(l+1) f_+^{(l)}(W) + l f_-^{(l)}(W) \right]_{ji} P_l(x), \tag{A2}$$

$$G_{ji}(W, x) = \sum_{l=1}^{\infty} \left[f_+^{(l)}(W) - f_-^{(l)}(W) \right]_{ji} P_l'(x). \tag{A3}$$

Restricting the orbital angular momentum up to the p-wave ($l = 1$), F and G can be written as

$$F_{ji}(W, x) = f^{(s)}(W) + x(2f_+^{(p)}(W) + f_-^{(p)}(W)), \tag{A4}$$

$$G_{ji}(W, x) = f_+^{(p)}(W) - f_-^{(p)}(W). \tag{A5}$$

Then, we make unitarizations to the amplitudes in the algebraic equation as [34]

$$f^{(s)}(W) = (1 - f^{(s)}_{\rm tree} g)^{-1} f^{(s)}_{\rm tree}, \tag{A6}$$

$$f^{(p)}_{+}(W) = (1 - f^{(p)}_{+\,\rm tree} g)^{-1} f^{(p)}_{+\,\rm tree}, \tag{A7}$$

$$f^{(p)}_{-}(W) = (1 - f^{(p)}_{-\,\rm tree} g)^{-1} f^{(p)}_{-\,\rm tree}. \tag{A8}$$

Here $f_{\rm tree}$ corresponds to the tree-level amplitude, giving the interaction kernel of the coupled channel. In this study, we use the Weinberg–Tomozawa term to $f^{(s)}_{\rm tree}$, as in Ref. [21]:

$$(f^{(s)}_{\rm tree})_{ij} = -C_{ij} \frac{1}{4f^2}(2W - M_i - M_j)\sqrt{\frac{M_i + E_i}{2M_i}}\sqrt{\frac{M_j + E_j}{2M_j}}, \tag{A9}$$

with the channel indices i and j, the baryon mass M, the meson decay constant $f = 1.123 f_\pi$ ($f_\pi = 93\,\text{MeV}$), and the baryon energy E. For $f^{(p)}_{\pm\,\rm tree}$, on the other hand, we choose the explicit Λ, Σ, and Σ^* Born terms, as in Eqs. (19)–(22) in Ref. [34]. The meson–baryon loop integral g in dimensional regularization is written as

$$\begin{aligned} g_l(W) &= i2M_l \int \frac{d^4q}{(2\pi)^4} \frac{1}{(P-q)^2 - M_l^2 + i\epsilon} \frac{1}{q^2 - m_l^2 + i\epsilon} \\ &= \frac{2M_l}{16\pi^2}\left\{ a_i(\mu) + \ln\frac{M_l^2}{\mu^2} + \frac{m_l^2 - M_l^2 + W^2}{2W^2}\ln\frac{m_l^2}{M_l^2} \right. \\ &\quad + \frac{\bar{q}_l}{W}[\ln(W^2 - (M_l^2 - m_l^2) + 2\bar{q}_l W) + \ln(W^2 + (M_l^2 - m_l^2) + 2\bar{q}_l W) \\ &\quad \left. - \ln(-W^2 + (M_l^2 - m_l^2) + 2\bar{q} W) - \ln(-W^2 - (M_l^2 - m_l^2) + 2\bar{q}_l W)] \right\}, \end{aligned} \tag{A10}$$

where m and M are the meson and baryon masses, respectively, μ is a regularization scale and a_i are subtraction constants in each of the isospin channels. Here we use same parameter as in Refs. [21] and [34]:

$$\begin{aligned} a_{\bar{K}N} &= -1.84, a_{\pi\Sigma} = -2.00, a_{\pi\Lambda} = -1.83 \\ a_{\eta\Lambda} &= -2.25, a_{\eta\Sigma} = -2.38, a_{K\Xi} = -2.67. \end{aligned} \tag{A11}$$

Using the meson–baryon scattering amplitudes in the chiral unitary approach, we can calculate the cross sections of $\bar{K}N$ to several channels. The cross sections are expressed as

$$\frac{d\sigma_{ij}}{d\Omega} = \frac{1}{16\pi^2}\frac{M_i M_j}{s}\frac{k'}{k}\left\{ |F_{ji}(W,x)|^2 + |G_{ji}(W,x)|^2 \sin^2\theta \right\}, \tag{A12}$$

with initial and final center-of-mass momenta k and k'.

Appendix B. Meson–baryon scattering amplitudes

In this appendix, we show a way to transform the amplitude obtained in the center-of-mass frame of the two-body meson–baryon system to the amplitude in the baryon rest frame. The idea is that we first obtain the invariant amplitude from the c.m. amplitude. Next we do the transformation of the invariant amplitude to the baryon rest frame.

Invariant amplitude of meson–baryon scattering

The Lorentz-invariant meson–baryon scattering amplitude of can be written in general in terms of two Lorentz-invariant functions, A and B:

$$T = \bar{u}(p_2)\,[A(s,t) + \gamma \cdot K\, B(s,t)]\, u(p_1), \tag{B1}$$

where p_1 and p_2 are the initial and final baryon momenta, respectively, the four-vector K is defined by $K = \frac{1}{2}(k_1 + k_2)$ with the initial and final meson momenta k_1 and k_2, and the Mandelstam variables s and t are given by $s = (p_1 + k_1)^2$ and $t = (k_1 - k_2)^2$.

Scattering amplitudes in the c.m. frame

In the c.m. frame, the scattering amplitudes are written as

$$T(W,x) = F(W,x) - iG(W,x)(\hat{k}_2 \times \hat{k}_1) \times \vec{\sigma}, \tag{B2}$$

with the partial wave decomposition

$$F(W,x) = \sum_{\ell=0}^{\infty} [(\ell+1) f_{\ell+}(W) + \ell f_{\ell-}(W)]\, P_\ell(x) \tag{B3}$$

$$G(W,x) = \sum_{\ell=1}^{\infty} [f_{\ell+}(W) - f_{\ell-}(W)]\, P'_\ell(x), \tag{B4}$$

where $W = \sqrt{s}$ is the c.m. energy and $x = \cos\theta$ with the scattering angle θ in the c.m. frame. The relation between (A, B) and (F, G) is given by

$$A = \frac{1}{2W}\left[\left(W + \frac{M_1 + M_2}{2}\right)\frac{F + xG}{a_1 a_2} + \left(W - \frac{M_1 + M_2}{2}\right)\frac{G}{b_1 b_2}\right] \tag{B5}$$

$$B = \frac{1}{2W}\left[\frac{F + xG}{a_1 a_2} - \frac{G}{b_1 b_2}\right], \tag{B6}$$

where $a = \sqrt{(E+M)/(2M)}$ and $b = \sqrt{(E-M)/(2M)}$ with the c.m. baryon energy E and baryon mass M.

Scattering amplitudes in the baryon rest frame

Let us consider the initial baryon at rest. The amplitude in this frame is given by

$$T = F'(W,x') - iG'(W,x')(\hat{k}'_2 \times \hat{k}'_1) \cdot \vec{\sigma}, \tag{B7}$$

where x' is the angle between $\vec{k}'_1$ and $\vec{k}'_1$.

The baryon rest frame amplitudes, F' and G', can be written in terms of the Lorentz-invariant amplitudes, A and B, as

$$F'(W,x') = a'_2\left[A(s,t) + \frac{1}{2}\left(\omega'_1 + \omega'_2 + \frac{|\vec{k}'_2|^2 - |\vec{k}'_1|^2}{E'_2 + M_2}\right)B(s,t)\right] \tag{B8}$$

$$G'(W,x') = -a'_2\frac{|\vec{k}'_1||\vec{k}'_2|}{E'_2 + M_2}B(s,t), \tag{B9}$$

where $a'_2 = \sqrt{(E'_2 + M_2)/(2M_2)}$ with the final baryon energy E'_2 in the initial baryon rest frame and the final baryon mass M_2.

The kinematical variables are expressed in terms of W and $\cos\theta'$ as

$$|\vec{k}_1'| = \frac{W|\vec{k}_1|}{M_1} \tag{B10}$$

$$\omega_1' = \gamma W - M_1 \tag{B11}$$

$$\omega_2' = \frac{\omega_2 + \beta\cos\theta'\sqrt{\omega_2^2 - \gamma^2 m_2^2(1-\beta^2\cos^2\theta')}}{\gamma(1-\beta^2\cos^2\theta')} \tag{B12}$$

$$|\vec{k}_2'| = \frac{\beta\cos\theta'\omega_2 + \sqrt{\omega_2^2 - \gamma^2 m_2^2(1-\beta^2\cos^2\theta')}}{\gamma(1-\beta^2\cos^2\theta')}. \tag{B13}$$

Substituting Eqs. (B5) and (B6) into Eqs. (B8) and (B9), we obtain

$$F'(W,x') = \frac{a_2'}{4W}\left[\left(2W + \omega_1' + \omega_2' + M_1 + M_2 + \frac{|\vec{k}_2'|^2 - |\vec{k}_1'|^2}{E_2' + M_2}\right)\frac{F(W,x) + xG(W,x)}{a_1 a_2}\right.$$
$$\left. + \left(2W - \omega_1' - \omega_2' - M_1 - M_2 - \frac{|\vec{k}_2'|^2 - |\vec{k}_1'|^2}{E_2' + M_2}\right)\frac{G(W,x)}{b_1 b_2}\right] \tag{B14}$$

$$G'(W,x') = -\frac{a_2'}{2W}\frac{|\vec{k}_1'|\,|\vec{k}_2'|}{E_2' + M_2}\left[\frac{F(W,x) + xG(W,x)}{a_1 a_2} - \frac{G(W,x)}{b_1 b_2}\right], \tag{B15}$$

where $x = \cos\theta$ and $x' = \cos\theta'$ with the angles between the mesons in the c.m. and baryon rest frames, respectively. These are related by the boost transformation:

$$\cos\theta = \frac{\gamma}{|\vec{k}_2|}(-\beta\omega_2' + |\vec{k}_2'|\cos\theta') = \eta + \xi x', \tag{B16}$$

where $\beta = |\vec{p}_1|/E_1$ and $\gamma = (1-\beta^2)^{-1/2}$.

The amplitudes $F'(W,x')$ and $G'(W,x')$ can be decomposed by a partial wave in the laboratory frame:

$$F'(W,x') = \sum_{\ell=0}^{\infty} F'^{(\ell)} P_\ell(x') = \sum_{\ell=0}^{\infty}\left[(\ell+1)f_{\ell+}'(W) + \ell f_{\ell-}'(W)\right]P_\ell(x') \tag{B17}$$

$$G'(W,x') = \sum_{\ell=1}^{\infty} G'^{(\ell)} P_\ell'(x') = \sum_{\ell=1}^{\infty}\left[f_{\ell+}'(W) - f_{\ell-}'(W)\right]P_\ell'(x'), \tag{B18}$$

where

$$F'^{(\ell)}(W) = \frac{2\ell+1}{2}\int_{-1}^{1} dx' F'(W,x')P_\ell(x') \tag{B19}$$

$$G'^{(\ell)}(W) = \frac{2\ell+1}{2\ell(\ell+1)}\int_{-1}^{1} dx'(1-x'^2)G'(W,x')P_\ell'(x'). \tag{B20}$$

Here we have used

$$\int_{-1}^{1} dx\, P_\ell(x)P_k(x) = \frac{2}{2\ell+1}\delta_{\ell k} \tag{B21}$$

$$\int_{-1}^{1} dx(1-x^2)P_\ell'(x)P_k'(x) = \int_{-1}^{1} dx\, P_\ell^1(x)P_k^1(x) = \frac{2}{2\ell+1}\frac{(\ell+1)!}{(\ell-1)!}\delta_{\ell k}. \tag{B22}$$

References

[1] R. H. Dalitz and S. F. Tuan, Phys. Rev. Lett. **2**, 425 (1959).
[2] R. H. Dalitz and S. F. Tuan, Ann. Phys. **10**, 307 (1960).
[3] N. Kaiser, P. B. Siegel, and W. Weise, Nucl. Phys. A **594**, 325 (1995).
[4] E. Oset and A. Ramos, Nucl. Phys. A **635**, 99 (1998).
[5] J. A. Oller and U. G. Meissner, Phys. Lett. B **500**, 263 (2001).
[6] M. F. M. Lutz and E. E. Kolomeitsev, Nucl. Phys. A **700**, 193 (2002).
[7] E. Oset, A. Ramos, and C. Bennhold, Phys. Lett. B **527**, 99 (2002); **530**, 260 (2002) [erratum].
[8] T. Hyodo, S. I. Nam, D. Jido, and A. Hosaka, Phys. Rev. C **68**, 018201 (2003).
[9] T. Hyodo, S. I. Nam, D. Jido, and A. Hosaka, Prog. Theor. Phys. **112**, 73 (2004).
[10] D. Jido, J. A. Oller, E. Oset, A. Ramos, and U. G. Meissner, Nucl. Phys. A **725**, 181 (2003).
[11] B. Borasoy, R. Nissler, and W. Weise, Eur. Phys. J. A **25**, 79 (2005).
[12] B. Borasoy, U.-G. Meissner, and R. Nissler, Phys. Rev. C **74**, 055201 (2006).
[13] T. Hyodo and D. Jido, Prog. Part. Nucl. Phys. **67**, 55 (2012).
[14] Y. Ikeda, T. Hyodo, and W. Weise, Phys. Lett. B **706**, 63 (2011).
[15] Y. Ikeda, T. Hyodo, and W. Weise, Nucl. Phys. A **881**, 98 (2012).
[16] T. Hyodo, D. Jido, and A. Hosaka, Phys. Rev. C **78**, 025203 (2008).
[17] T. Hyodo, A. Hosaka, M. J. Vicente Vacas, and E. Oset, Phys. Lett. B **593**, 75 (2004).
[18] M. F. M. Lutz and M. Soyeur, Nucl. Phys. A **748**, 499 (2005).
[19] V. K. Magas, E. Oset, and A. Ramos, Phys. Rev. Lett. **95**, 052301 (2005).
[20] L. S. Geng, E. Oset, and M. Doring, Eur. Phys. J. A **32**, 201 (2007).
[21] D. Jido, E. Oset, and T. Sekihara, Eur. Phys. J. A **42**, 257 (2009).
[22] D. Jido, E. Oset, and T. Sekihara, Eur. Phys. J. A **47**, 42 (2011).
[23] D. Jido, E. Oset, and T. Sekihara, arXiv:1207.5350 [nucl-th].
[24] J. Esmaili, Y. Akaishi, and T. Yamazaki, Phys. Rev. C **83**, 055207 (2011).
[25] O. Braun et al., Nucl. Phys. B **129**, 1 (1977).
[26] H. Noumi et al., J-PARC proposal E31: Spectroscopic study of hyperon resonances below $\bar{K}N$ threshold via the (K^-, n) reaction on deuteron (2009).
[27] K. Miyagawa and J. Haidenbauer, Phys. Rev. C **85**, 065201 (2012).
[28] T. Yamazaki and Y. Akaishi, Phys. Lett. B **535**, 70 (2002).
[29] D. Jido and Y. Kanada-En'yo, Phys. Rev. C **78**, 035203 (2008).
[30] A. Gal and H. Garcilazo, Phys. Rev. D **78**, 014013 (2008).
[31] K. Nakamura et al. [Particle Data Group Collaboration], J. Phys. G: Nucl. Part. Phys. **37**, 075021 (2010).
[32] M. Lacombe, B. Loiseau, R. Vinh Mau, J. Cote, P. Pires, and R. de Tourreil, Phys. Lett. B **101**, 139 (1981).
[33] R. Machleidt, Phys. Rev. C **63**, 024001 (2001).
[34] D. Jido, E. Oset, and A. Ramos, Phys. Rev. C **66**, 055203 (2002).
[35] Center of Nuclear Study (Available at: http://gwdac.phys.gwu.edu/.)
[36] J. C. Nacher, E. Oset, H. Toki, and A. Ramos, Phys. Lett. B **455**, 55 (1999).
[37] M. Niiyama et al., Phys. Rev. C **78**, 035202 (2008).
[38] K. Moriya and R. Schumacher [CLAS Collaboration], Nucl. Phys. A **835**, 325 (2010).